**INVITED PAPER**

*M. Okamoto**

*Advanced Polymeric Materials Engineering, Graduate School of Engineering Toyota Technological Institute, Nagoya, Japan*

# Polymer/Layered Silicate Nano-composites

## Structure Development and Processing Operations

*Polymer/layered filler nano-composites (PLFNCs) offer remarkably improved mechanical properties with low inorganic filler loading. Major developments in this field have been carried out over the last one and half decades. However, we are far from the goal of understanding the mechanisms of the enhancement effects in nanocomposites. Continued progress in nanoscale control, as well as an improved understanding of the physicochemical phenomena at the nanometer scale, has contributed to the rapid development of novel PLFNCs. We describe nano-structure development and processing operations in PLFNCs.*

### 1 Introduction

A decade of research has shown that nanostructured materials have the potential to significantly impact growth at every level of the world economy in the 21st century. This new class of materials is now being introduced in structural applications including gas barrier film and flame retardant products, and load-bearing applications.

Of particular interest is recently developed *nano-composites* consisting of a polymer and layered silicate that often exhibit remarkably improved properties [1] when compared with polymer or conventional composites (both micro- and macro-composites). In polymer/layered silicate nano-composites, a PA 6/layered silicate hybrid [2] reported by Toyota Central Research & Development Co. Inc. (TCRD) was successfully prepared by *in-situ* polymerization of ε-caprolactam in a dispersion of montomorrillonite (MMT). The silicate can be dispersed in liquid monomer or a solution of monomer. It is also possible to melt-mix polymers with layered silicates, avoiding the use of organic solvents. The latter method permits the use of conventional processing techniques such as injection molding and extrusion. The extensive literature in nano-composite research is covered in recent reviews [1, 3, 4].

Continued progress in nanoscale control, as well as an improved understanding of the physicochemical phenomena at the nanometer scale, has contributed to the rapid development of novel nano-composites. This presents current research on polymer/layered filler nano-composites (PLFNCs) with the primary focus on nano-structure development and processing operations.

* Mail address: M. Okamoto, Advanced Polymeric Materials Engineering, Graduate School of Engineering, Toyota Technological Institute, 2-12-1 Hisakata, Tempaku, Nagoya 468 8511, Japan
E-mail: okamoto@toyota-ti.ac.jp, Morand Lambla Award 2005 recipient.

### 2 Nano-structure Development

#### *2.1 Historical Point of View*

Earlier attempts of preparing polymer/layered filler composites are found in almost half-a-century old patent literature [5, 6]. In such cases, incorporation of 40 to 50 wt.% clay mineral (bentonite, hectorite, etc.) into a polymer was attempted, but ended with unsatisfactory results. The maximum modulus enhancement was only around 200 %, although the clay loading was as much as 50 wt.%. The failure was due to the dispersion of clay particles in the matrix, in which silicate minerals existed as agglomerated tactoids. Such a poor dispersion of the silicate particles could improve the material rigidity, but not strength, elongation at break and toughness [5, 6].

A prime reason for the tactoids dispersion into well-dispersed exfoliated monolayers of the silicate is due to the intrinsic incompatibility of hydrophilic layered silicates with hydrophobic engineering plastics. One attempt at circumventing this difficulty was made by Unitika Ltd. [7] about 30 years ago in preparing PA 6/layered silicate composites (not nano-composites) *via in situ* polymerization of ε-caprolactam with MMT.

The first major breakthrough of the problem was brought around 1987, when Fukushima and Inagaki of TCRD, *via* their detailed study on polymer/layered silicate composites, persuasively demonstrated that lipophilization by replacing inorganic cations in galleries of the native clay with alkylammonium surfactant (*intercalant*) successfully made them compatible with hydrophobic polymer matrices [8]. The modified clay was thus called lipophilized clay, organo-phillic clay or simply organoclay. Furthermore, they found that the lipophilization enabled to expand silicate nano-galleries and to exfoliate the silicate layers into single layers of a nanometer thickness.

*Usuki, Fukushima* and their colleagues successfully prepared, for the first time, exfoliated PA 6/MMT hybrid *via in-situ* polymerization of ε-caprolactam, in which alkylammonium-modified MMT was thoroughly dispersed in advance [2, 9].

Intercalation of small molecules into silicate galleries has been found by researchers when studying Mayan archeological sites [10]. Maya blue was used in Mesoamerica and colonial Mexico as late as the 20th century. Maya blue color is resistant to diluted mineral acids, alkalis, moderate heat and even biocorrosion. This blue color contains clay (mainly MMT clay and palygorskite ($Mg_5(Si,Al)_8O_{20}(OH)_28H_2O$)) and indigo molecules ($C_{16}H_{10}N_2O_2$). Intercalation of indigo molecules into MMT galleries and/or encapsulation in the pores of palygorskite might explain the observed resistance to degradation in the extreme conditions of the rain forest (see Fig. 1).

A)

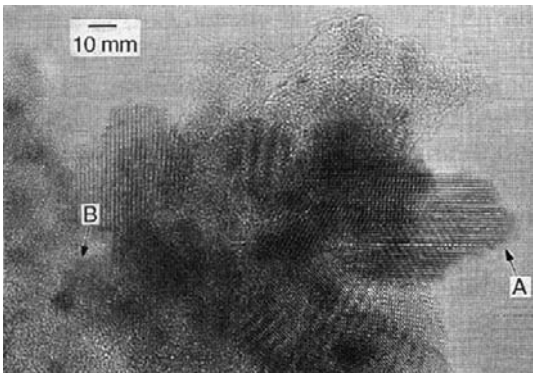


B)

*Fig. 1. Maya blue was used in this mural representing a solider from Msoamerica (A), needle shape of the palygorskite crystals [10] (B)*

### *2.2 Melt Intercalation*

Since the possibility of direct melt intercalation was first demonstrated [11], melt intercalation has become the main preparation route for intercalated polymer/layered silicate nano-composites. This process involves annealing, statically or under shear, a mixture of the polymer and organically modified layered fillers (OMLFs) above the softening point of the polymer. During annealing, the polymer chains diffuse from the bulk polymer melt into the nano-galleries between the layered fillers.

In order to understand the thermodynamic issue associated with the nano-composites formation, *Vaia* et al. have applied mean-field statistical lattice model and found conclusions based on the mean field theory nicely agreed with the experimental results [12, 13]. The entropy loss associated with confinement of a polymer melt is not prohibited to nanocomposite formation because an entropy gain associated with the layer separation balances the entropy loss of polymer intercalation, resulting in a net entropy change near to zero. Thus, from the theoretical model, the outcome of nano-composite formation via polymer melt intercalation depends on energetic factors, which may be determined from the surface energies of the polymer and OMLF.

Nevertheless, we have often faced the problem that the nano-composite shows fine and homogeneous distribution of the nano-particles in the polymer matrix (e. g., poly(L-lactide)) without any clear peak shifts of the mean interlayer spacing of the (001) plane as revealed by wide-angle X-ray diffraction (WAXD) analysis [14]. Furthermore we sometimes encounter a decreasing of the interlayer spacing compared with that of pristine OMLF, despite very fine dispersion of the silicate particles. To the best of our knowledge, the mechanism of the direct melt intercalation in the nano-composite formation is not very well explored in the literature. For this reason, information on the structure of the surfactant (intercalant)-polymer interface is necessary to understand the intercalation kinetics that can predict final nano-composite morphology and overall material properties.

### *2.3 Interlayer Structure of OMLFs and Intercalation*

*Lagaly* has suggested the paraffin-type layer structure of the intercalants in the case of highly surface charged clay minerals [15]. This model was derived from WAXD analysis assuming all-trans conformation of the intercalants. *Vaia* et al. [16] have shown that alkyl chains can vary from liquid-like to solid-like, with the liquid-like structure dominating as the interlayer density or chain length decreases, or as the temperature increases. They used Fourier transform infrared spectroscopy (FTIR), which is sensitive to the *gauche*/*trans* conformer ratio in alkyl chains and the lateral chain-chain interactions. In addition, for the longer chain length intercalants, the intercalants in the layered silicate can show thermal transition akin to melting or liquid-crystalline to liquid like transitions upon heating. The gauche content was found to decrease with increasing intercalant concentration. The chains adopt an essentially all-trans conformation when intercalant concentration is high (more than cation-exchange capacity (CEC)) [17]. More recently, *Osman* [18] reported that the all-trans conformation of the alkyl chains was preferentially adopted when using highly surface charge density clay (vermiculite).

On the other hand, *Paul* et al. [19] used molecular simulations and reported disordered conformation of the alkyl chains (containing hydroxyl-ethyl units) with a tendency for laying to the silicate surfaces. A systematic investigation is required using OMLFs having different types of intercalant and nano-fillers with different surface charge density. Furthermore, the investigation of the correlation between the intercalant-polymer interface and the melt intercalation has been still sparse. A better understanding of the correlation and subsequent preparation of the nano-composites are of fundamental importance in controlling the nanoscale structure.

*Okamoto* et al. [20] reported that the interlayer structure on OMLFs with respect to the number per area (surface charge density) and size of intercalant chains for nano-composite formation. In the study they presented an interdigitated layer structure model of the OMLF, where the intercalants are oriented with some inclination to the host layer in the interlayer space. Details regarding this model and explanation are presented in [19]. The illustration of a model of interlayer structure of some intercalant (*n*-hexadecyl tri-*n*-butyl phosphonium cation: $C_{16}TBP^{+}$) in gallery space of layered titanate (HTO: $H_{1.07}Ti_{1.73}O_{3.95} \cdot 0.5\,H_2O$) is shown in Fig. 2. For nano-fillers with highly surface charge density ($1.26e^{-}/nm^2$, see Table 1), the intercalants can adopt a configuration with orientation where the alkyl chains (with all-trans conformation) are tilted under the effect of the van der Waals forces, which decreases

the chain-to-chain distance. For this reason the angle α should be directly related to the packing density of the alkyl chains. The value of α decreases until close contact between the chains is attained, giving an increasing degree of the crystallinity of the intercalants into the nano-galleries.

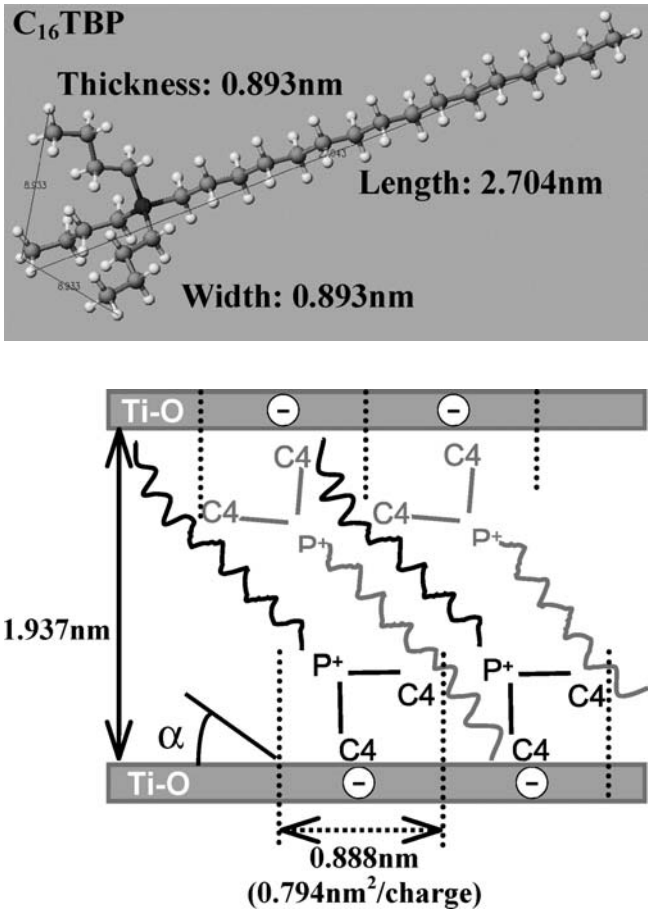


*Fig. 2. Illustration of a model of interlayer structure of intercalant n-hexadecyl tri-n-butyl phosphonium cation ($C_{16}$TBP) in gallery space of layer titanate (HTO). The average distance between exchange sites is 0.888 nm calculated by surface charge density of 1.26 $e^-/nm^2$. For $C_{16}$TBP, obtained molecular length, thickness and width are 2.704 nm, 0.89 nm and 0.89 nm, respectively (see upper panel). The tilt angle α of the intercalants can be estimated by the combination of the interlayer spacing, molecular dimensions and loading amount of intercalants when the alkyl chains are adopted all-trans comformation [20]*

*Okamoto* et al. also investigated the intercalation behavior of diphenyl sulfide (DFS) molecules into nano-galleries based on OMLFs (see Fig. 3) [20]. One can observe the strong correlation between initial interlayer opening (which is estimated after subtraction of the layer thickness) and layer expansion (= Δ opening) after mixing with DFS, regardless of the miscibility between intercalant and DFS. That is, the smaller initial opening leads to the larger interlayer expansion. In other words, the smaller interlayer opening caused by the lower surface charge density and/or short chain length of the intercalant (e. g., $qC_{14}$(OH) and $C_{12}$TPP) promotes the large amount of intercalation of DFS molecules.

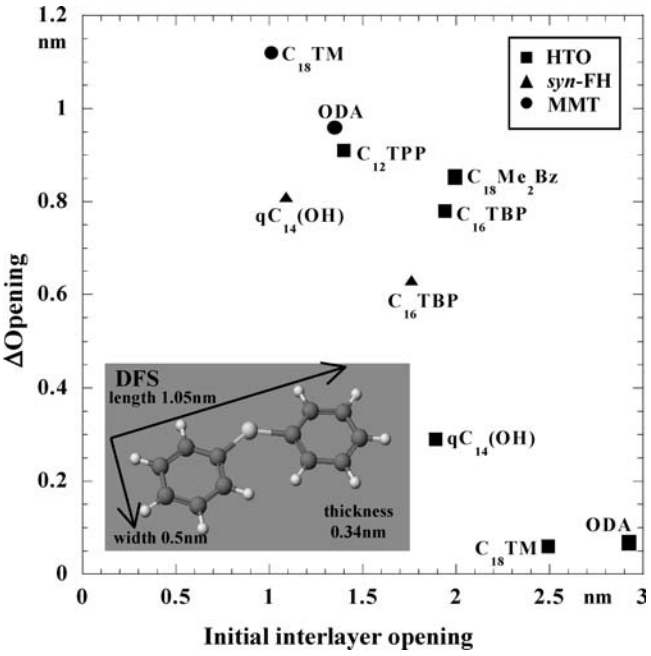


*Fig. 3. Plot of initial interlayer opening versus Δ opening for various OMLFs intercalated with DFS. The insert shows molecular dimensions of DFS calculated using a molecular dinamic program (MM2 in Quantum CAChe, Fujitsu Ltd.), taking van der Waales radi into consideration. n-octyl triphenyl phosphonium ($C_{12}$TPP), N-(cocoalkyl)-N,N-[bis(2-hydroxyethyl)]-N-methyl ammonium ($qC_{14}$(OH)), and octadecyl benzyl di-methyl ammonium ($C_{18}Me_2Bz$) cations are miscible with DFS as revealed by melting temperature depression of DFS, while octadecylammonium (ODA), octadecyl tri-methylammonium ($C_{18}$TM) cations are immiscible with DFS*

| Parameters | HTO | *syn*-FH | MMT |
|---|---|---|---|
| Chemical formula | $H_{1.07}Ti_{1.73}O_{3.95} \cdot 0.5\,H_2O$ | $Na_{0.66}Mg_{2.6}Si_4O_{10}(F)_2$ | $Na_{0.33}(Al_{1.67}Mg_{0.33})\,Si_4O_{10}(OH)_2$ |
| Particle size (nm) | ~100–200 | ~100–200 | ~100–200 |
| BET area ($m^2$/g) | ~2400 | ~800 | ~700 |
| CEC[a] (meq/100g) | ~200 (660) | ~120 (170) | ~90(90) |
| $e^-$/charge($nm^2$) | 1.26 | 0.971 | 0.708 |
| Density (g/$cm^3$) | 2.40 | 2.50 | 2.50 |
| Refractive index ($n_D^{20}$) | 2.3 | 1.55 | 1.55 |
| pH | 4–6 | 9–11 | 7.5–10 |

[a] Methylene blue adsorption method. The values in the parenthesis are calculated from chemical formula of nano-fillers

*Table 1. Characteristic parameters of nano-fillers [20]*

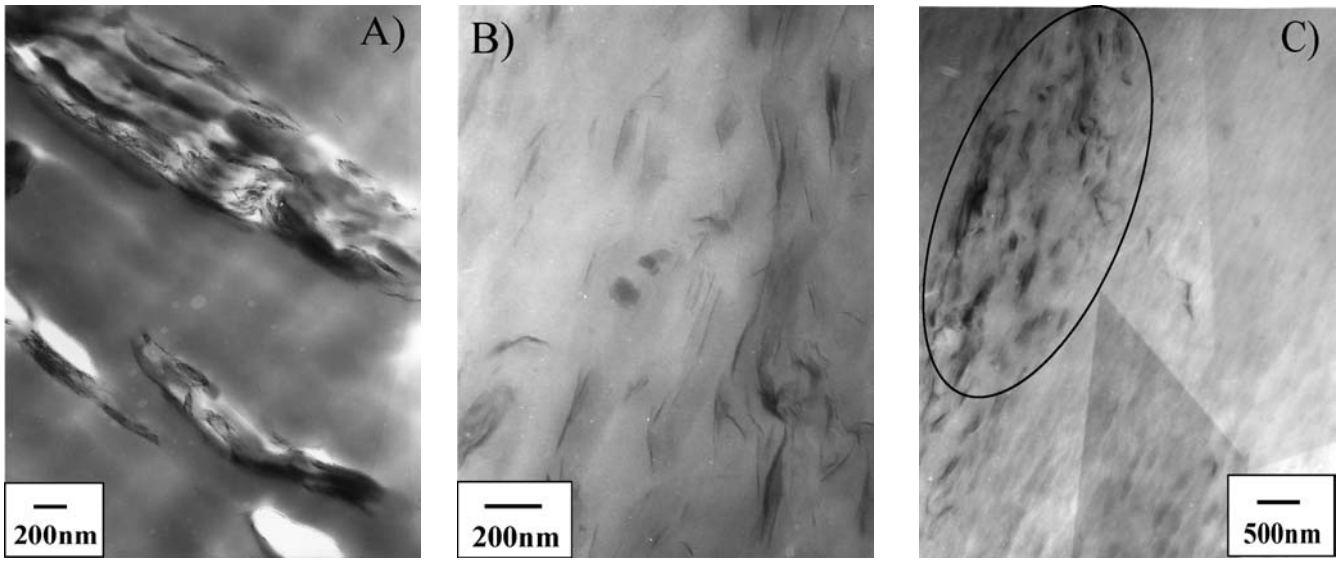


*Fig. 4. Bright filed TEM images of (A) PPS/syn-FH-$C_{16}$TBP, (B) and (C) PPS/MMT-$C_{16}$TBP prepared by annealing at 300 °C for 30 s (without shear processing). The dark entities are the cross section and/or face of intercalated-and-stacked silicate layers, and the bright areas are the matrix. The circled area indicates the aggregated particles contains many discrete silicate layers with fine dispersion [21]*

For HTO-ODA intercalated with DFS (HTO-ODA/DFS) and HTO-$C_{18}$TM/DFS, the absolute value of Δ opening (0.07 nm (2.4 %) and 0.06 nm (2.4 %), respectively) is lower than the molecular dimension of DFS (length, width and thickness are 1.05 nm, 0.5 nm and 0.34 nm, respectively) (see the insert in Fig. 3). This suggests that the DFS molecules can not penetrate into galleries if we compare the apparent interlayer expansion (= Δ opening). It is necessary to understand the meaning of the interlayer expansion in the intercalation estimated by WAXD analysis. This interdigitated structure may imply the different orientation angle that the intercalants can adopt when DFS molecules penetrate into the galleries. Apparently, the interdigitated layer structure provides a balance between DFS penetration and different orientation angle of the intercalants. From this result, the entropic contribution of the intercalants, which leads to the entropy gain associated with the layer expansion after intercalation of the small molecules and/or polymer chains, may not be significant due to the interdigitated layer structure. Presumably the penetration takes place by pressure drop within the nano-galleries, nano-cappillary action, generated by the two platelets.

This interdigitated structure model is suitable to explain the differences in the polymer intercalation behavior between different OMLFs. Without shear processing, *Okamoto* et al. have successfully prepared poly(*p*-phenylenesulfide) (PPS)-based nano-composite using optimal interlayer structure on OMLF (see Fig. 4). The large agglomerated tactoids of about 300 nm thickness are seen in Fig. 4A, when using synthetic fluorine hectorite (*syn*-FH) modified with $C_{16}$TBP. On the other hand, Figs. 4B and C show both larger views permitting the observation of discrete silicate layers, when using MMT modified with $C_{16}$TBP. The aggregated feature of the silicate layers is also observed in Fig. 4C. However, an aggregated particle contains many discrete silicate layers with finer dispersion. For PPS/MMT-$C_{16}$TBP, prepared by annealing without shear processing, the penetration of PPS chains promotes the delamination of the stacked MMT layers. The delamination of the stacked nano-fillers was governed by the initial interlayer opening, whereas the uniform dispersion of the nano-fillers was affected by the shear processing [21].

Compared to OMLFs, a nano-composite structure is difficult to model using atomic scale molecular dynamics (MD) because the intercalated polymer chain conformation is complex and can hardly be in the equilibrium state. However, *Pricl* et al. [22] explored and characterized the atomic scale structure to predict binding energies and basal spacing of PLFNCs based on polypropylene (PP) and maleated (MA) PP (PP-MA), MMT, and different alkylammonium ions as intercalants (see Fig. 5). From a global interpretation of all these MD simulation results, they concluded that intercalants with smaller volume are more effective for clay modification as they improve the thermodynamics of the system by increasing the binding energy. On the other hand, intercalants with longer tails are more effective for intercalation and exfoliation processes, as they lead to higher basal spacing. Additional information is necessary to predict more reasonable nano-structure of PLFNCs; some literatures [23 to 26] related to the confined polymer chains within the silicate galleries by using coarse-grained MD simulation appeared.

### *2.4 Novel Compounding Process*

Complete exfoliation of the OMLFs is not feasible after melt intercalation, although appropriate shear is applied during melt compounding. Recently, an *in-situ* polymerization method used supercritical $CO_2$ (sc-$CO_2$) as a processing aid to achieve a uniform distribution in a PLFNC at high MMT clay loading (~ 40 wt.%) [27]. *Zhao* et al. [28] presented unambiguous evidence for sc-$CO_2$-mediated intercalation of poly(ethylene oxide) (PEO) into $Na^+$-MMT compared with polymer intercalation in solution (water), in which an entropy-driven process is dominant. They successfully intercalated PEO into clay via a sc-$CO_2$-mediated process, a mechanism probably similar to

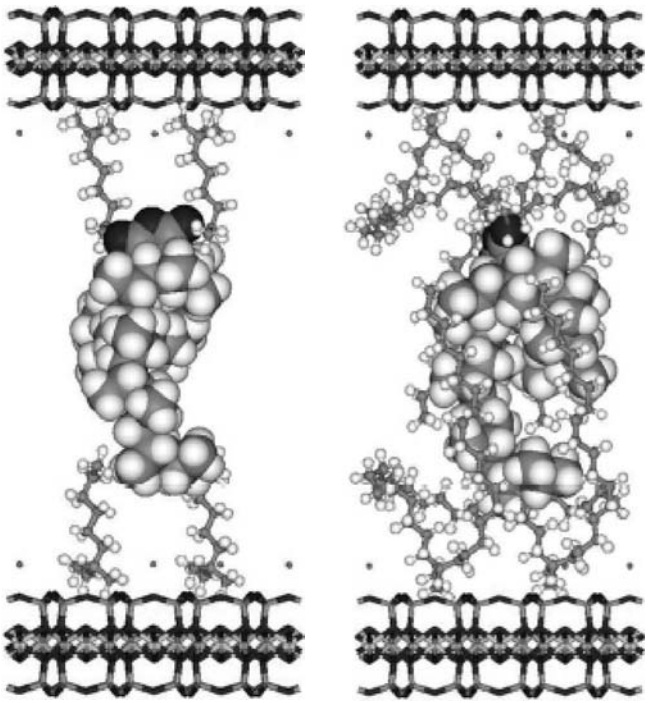

A) B)

*Fig. 5. Three component model used for basal spacing simulations, consisting of two layers of MMT with $K^+$ cations (stick model), four molecules of trimethylammonium cation (A) or dimethylstearylammonium cation (B) (stick and ball model), and one molecule of maleated PP (PP-MA) (ball model) [22]*

that found in polymer melts. Therefore, the sc-$CO_2$-mediated intercalation is an enthalpically driven process, deriving from a favorable intercalation between PEO and MMT. sc$CO_2$-mediated process is also conducted during melt compounding process. *Ozisik* et al. [29] examined the effect of the sc-$CO_2$ fed to the tandem extruder on the dispersion of OMLFs with different intercalants into a PA 6 matrix. In the absence of sc-$CO_2$, pressure improved the MMT clay delamination by reducing the free volume of the polymer and increasing the interaction between chains and ultimately increasing the viscosity. Using sc-$CO_2$ did not improve the clay dispersion due to the decreasing melt viscosity.

Another interesting approach for the delamination of OMLFs is an ultrasound in the preparation of PLFNCs. *Lee* et al. [30] reported the effect of the *in-situ* ultrasound on the polymer/MMT melt phase. They found an effective method to enhance the dispersion, intercalation and exfoliation of OMLFs in thermoplastic-based nano-composites. The same experiment was done by *Guo* et al. [31] for PP-base nano-composite preparation. The schematic representation of this technology is shown in Fig. 6. The maximum power output and frequency of the ultrasonic generator are 300 W and 20 kHz, respectively. They described the fine dispersion of silicate layers in PP matrix after ultrasonic treatment (100 W). However, the ultrasonic oscillations exhibited little effect on the delamination of OMLFs as revealed by transmission electron microscopy (TEM) observation.

Thus, the compounding with an assist from sc-$CO_2$ fluids and ultra-sonication did not improve the state of the nano-filler

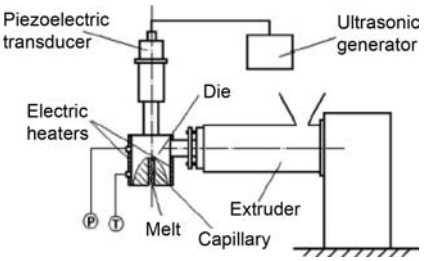


*Fig. 6. Schematic diagram of ultrasonic oscillations extrusion system [31]*

dispersion once a critical morphology was established. We have to develop more innovative compounding processes, especially in the preparation of the nano-composites possessing exfoliated layered fillers. Despite its physical importance, the pressure drop ($\Delta p$) within the nano-galleries [20], which makes the polymer penetration more difficult, has not yet been discussed fully.

Another challenge is the exfoliation of talc fillers by solid-state shear processing using the pan-type mill to prepare PP/talc nano-composites [32]. Although the delamination of talc fillers was not achieved in the nano-composite as revealed by TEM images, no indication of the layer correlation was observed in WAXD profiles. Solid-state shear processing may be an innovative technique to delaminate the layered fillers.

## 3 Flow-induced Structure Development

Rheological behavior, especially elongational and shear flow behavior in the molten state of PLFNCs have not well been known, although such knowledge should be indispensable in relation with their performance in processing operations. One objective of this review is to focus on a profound understanding of PLFNCs for their innovations in practical material production. For this purpose, it is indispensable to illuminate the nano-structure as well as rheological properties of PLFNCs to assess appropriate processing conditions for designing and controlling their hierarchical nano-structure, which must be closely related with their material performance.

### *3.1 Elongational Flow and Strain-induced Hardening*

*Okamoto* et al. [33] first conducted elongation test of PP-based nano-composites (PPCN4) in molten state at constant Hencky strain rate, $\dot{\varepsilon}_0$ using an elongation flow opto-rheometry, and attempted to control the alignment of the dispersed MMT layers with nanometer dimensions of an intercalated PPCNs under uniaxial elongational flow.

Fig. 7 shows double logarithmic plots of transient elongational viscosity $\eta_E(\dot{\varepsilon}_0; t)$ against time t observed for PA 6/OMLF system (N6CN3.7: MMT = 3.7 wt.%) and PPCN4 (MMT = 4 wt.%)) with different Hencky strain rates $\dot{\varepsilon}_0$ ranging from 0.001 $s^{-1}$ to 1.0 $s^{-1}$. The solid curve represents time development of three-fold shear viscosity, $3\eta_0(\dot{\gamma}; t)$, at 225 °C with a constant shear rate $\dot{\gamma} = 0.001\ s^{-1}$. In $\eta_E(\dot{\varepsilon}_0; t)$ at any $\dot{\varepsilon}_0$, N6CN3.7 melt shows a weak tendency of *strain-induced*

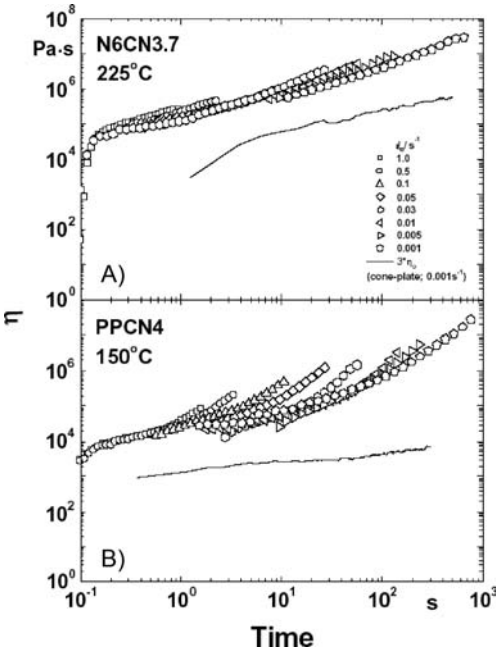


*Fig. 7. Time variation of elongational viscosity $\eta_E(\dot{\varepsilon}_0; t)$ for (A) N6CN3.7 melt at 225 °C and for (B) PPCN4 at 150 °C. The solid line shows three times the shear viscosity, $3\eta_E(\dot{\gamma}; t)$, taken at a low shear rate $\dot{\gamma} = 0.001\ s^{-1}$ on a cone-plate rheometer [34]*

*hardening* as compared to that of PPCN4 melt. A strong behavior of strain-induced hardening for PPCN4 melt originated from the perpendicular alignment of the silicate layers to the stretching direction as reported by *Okamoto* et al. [34].

From TEM observation [35], the N6CN3.7 forms a fine dispersion of the silicate layers of about 100 nm in $L_{clay}$, 3 nm thickness in $d_{clay}$ and $\xi_{clay}$ of about 20 to 30 nm between them. The $\xi_{clay}$ value is a one order of magnitude lower than the value of $L_{clay}$, suggesting the formation of spatially-linked like structure of the dispersed clay particles in PA 6 matrix. For N6CN3.7 melt, the silicate layers are so densely dispersed into the matrix and hence difficult to align under elongational flow. Under flow fields, the silicate layers might translationally move, but not rotationally in such a way that the loss energy becomes minimum. This tendency was also observed in PPCN7.5 melt having higher content of MMT (= 7.5 wt.%) [36].

One can observe two features for the shear viscosity curve. First, the extended Trouton rule, $3\eta_0(\dot{\gamma}; t) \cong \eta_E(\dot{\varepsilon}_0; t)$, does not hold for both N6CN3.7 and PPCN4 melts, as opposed to the melt of ordinary homo-polymers. The latter, $\eta_E(\dot{\varepsilon}_0; t)$, is more than 10 times larger than the former, $3\eta_0(\dot{\gamma}; t)$. Second, again unlike ordinary polymer melts, $3\eta_0(\dot{\gamma}; t)$ of N6CN3.7 melt increases continuously with t, never showing a tendency of reaching a steady state within the time span (600 s or longer) examined here. This *time-dependent thickening* behavior may be called *anti-thixotropy* or *rheopexy*. Under slow shear flow ($\dot{\gamma} = 0.001\ s^{-1}$), $3\eta_0(\dot{\gamma}; t)$ of N6CN3.7 exhibits a much stronger rheopexy behavior with almost two order of magnitude higher than that of PPCN4. This reflects a fact that the shear-induced structural change involved a process with an extremely long relaxation time as well as for other PLFNCs having rheopexy behavior [37], especially under the weak shear field.

### *3.2 Alignment of Silicate Layers*

The orientation of silicate layers and PA 6 crystallites in injection molded N6CN using WAXD and TEM is examined [38, 39]. Kojima and his colleagues have found three regions of different orientations in the sample as a function of depth. Near the middle of the sample, where the shear forces are minimal, the silicate layers are oriented randomly and the PA 6 crystallites are perpendicular to the silicate layers. In the surface region, shear stresses are very high, so both the clay layers and the PA 6 crystallites are parallel to the surface. In the intermediate region, the clay layers, presumably due to their higher aspect ratio, still orient parallel to the surface and the PA 6 crystallites assume an orientation perpendicular to the silicate. Very recently, *Medellin-Rodriguez* et al. [40] reported that the molten N6CN samples showed planar orientation of silicate layers along the flow direction, which is strongly dependent on shear time as well as clay loading, reaching a maximally orienting level after being sheared for 15 min with $\dot{\gamma} = 60\ s^{-1}$.

*Okamoto* et al. have conducted TEM observations of the sheared N6CN3.7 with $\dot{\gamma} = 0.0006\ s^{-1}$ for 1000 s [34]. The edges of the silicate layers laying along the z-axis (marked with the arrows (A)) or parallel alignment of the silicate edges to the shear direction (x-axis) (marked with the arrows (B)) rather than assumingly random orientation in the PA 6 matrix are observed, but in fact, one cannot see these faces in this plane (Fig. 8). Here, it should be emphasized that the planar orientation of the silicate faces along the x–z plane does not take place prominently. For the case of rapid shear flow, the commonly applicable conjecture of the planar orientation of the silicate faces along the shear direction first demonstrated to be true by *Kojima* et al. [38].

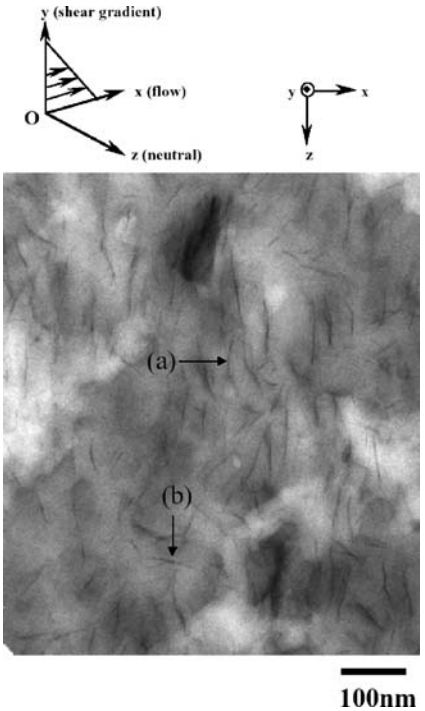


*Fig. 8. TEM micrograph in the x-z plane showing N6CN3.7 sheared at 225 °C with $\dot{\gamma} = 0.0006\ s^{-1}$ for 1000 s. The x-, y- and z-axes correspond respectively to flow, shear gradient and neutral direction [34]*

In uniaxial elongational flow (converging low) for a PPCN4, the formation of *a house-of-cards* structure is found by TEM analysis [33]. The perpendicular (but *not* parallel) alignment of disk-like MMT clay particles with large anisotropy toward the flow direction might sound unlikely but this could be the case especially under an elongational flow field, in which the extentional flow rate is the square of the converging flow rate along the thickness direction, if the assumption of *affine* deformation without volume change is valid. Obviously under such conditions, energy dissipation rate due to viscous resistance between the disk surface and the matrix polymer is minimal, when the disks are aligned perpendicular to the flow direction.

Moreover, *Lele* and his colleagues [41] recently reported the *in situ* rheo-X-ray investigation of flow-induced orientation in syndiotactic PP/layered silicate nanocomposite melt.

*In-situ* X-ray diffraction experiment during shear provided direct evidence of the rheology-structure effect in the materials. The agglomerated tactoids of MMT layers are oriented by shear and a high degree of orientation can be achieved after the yield transition.

Very recently, *Bafna* et al. [42] developed a technique to determine the three-dimensional (3D) orientation of various hierarchical organic and inorganic structures in PLSNCs. They studied the effect of compatibilizer concentration on the orientation of various structures in PLSNCs using 2D small angle X-ray scattering (SAXS) and 2D WAXD in three sample/camera orientations. Reflections and orientation of six different structural features were easily identified: (a) clay clusters/tactoids (0.12 μm), (b) modified/intercalated clay stacking period (002) (2.4 to 3.1 nm), (c) stacking period of unmodified clay platelets (002) (1.3nm), (d) clay (110) and (020) planes, normal (b) and (c), (e) polymer crystalline lamellae (001)(19−26nm), long period ((001) is an average crystallographic direction), and (f) polymer unit cell (110) and (200) planes. The corresponding identified reflections are presented in Fig. 9. A 3D study of the relative orientation of the above-mentioned structures was carried out by measuring three projections of each sample. Quantitative data on the orientation of these structural units in the nanocomposite film was determined through calculations of the major axis direction cosines and through a ternary, direction-cosine plot called a "Wilchinsky triangle" [43], previously proposed in lamellar orientation studies [44]. It allows a direct comparison of average preferred orientations for different structural features. In this way it is conceptually more useful than stereographic projections involving orientation density maps for a single WAXD reflection.

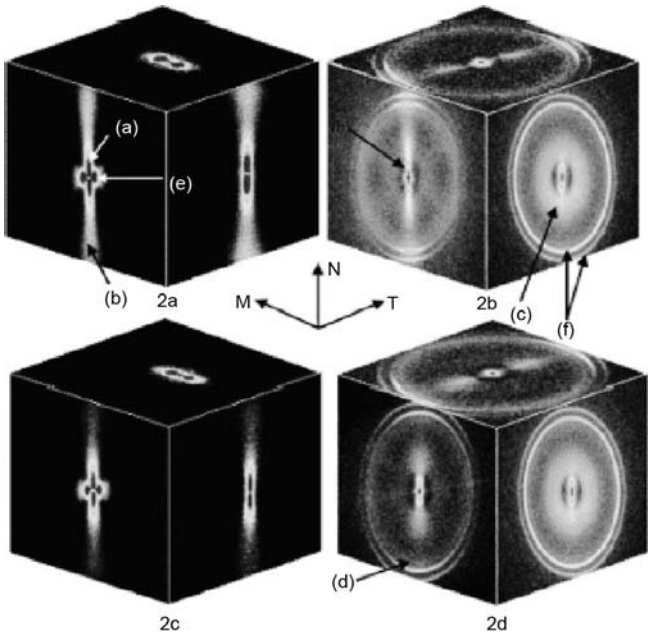


*Fig. 9. 2D SAXS (a and c) and WAXS (b and d) patterns for orientation MN (left face), NT (right face) and MT (top face) of films HD603 (a and b) and HD612 (c and d). The numbers in the parenthesis represent the reflections from the following: (a) clay tactoids, (b) modified/intercalated clay (002) plane, (c) unmodified clay (002) plane, (d) clay (110) and (020) plane, (e) polymer crystalline lamellar, (f) polymer unit cell (110) plane (inner ring) and (200) plane (outer ring) [42]*

Some 20 years ago *van Olphen* [45] pointed out that the electrostatic attraction between the layers of natural clay in aqueous suspension arises from higher polar force in the medium. The intriguing features such as yield stress thixotropy and/or rheopexy exhibited in aqueous suspensions of natural clay minerals may be taken as a reference to the present PLFNCs.

## 4 Processing Operations

Flow-induced internal structural change occurs in both shear and elongational flow, but differs between these flows, as judged from the above results on $\eta_E(\dot{\varepsilon}_0; t)$ and $3\eta_0(\dot{\gamma}; t)$ (see Fig. 7). Thus, with the rheological features of the PLFNCs and the characteristics of each processing operation, the tactics which should be selected for a particular nanocomposite for the enhancement of its mechanical properties.

For example, the strong strain-induced hardening in $\eta_E(\dot{\varepsilon}_0; t)$ is requisite for withstanding the stretching force during the processing, while the rheopexy in $3\eta_0(\dot{\gamma}; t)$ suggests that for such PLFNC a promising technology is the processing in confined space such the injection molding where shear force is crucial.

### *4.1 Foam Processing Using sc-$CO_2$*

The first successful nanocomposite foam, processed by using supercritical $CO_2$ as a physical foaming agent, appeared through a pioneering effort by *Okamoto* et al. [46, 47]. A small amount of nano-fillers in the polymer matrix serve as nucleation sites to facilitate the bubble nucleation during foaming. Novel nano-composite foams based on the combination of new nano-fillers and sc-$CO_2$ lead to a new class of the materials.

Fig. 10 shows the typical results of SEM images of the fracture surfaces of the intercalated polycarbonate (PC)-based nanocomposites (PCCNs) and PC/SMA blend (matrix) without clay foamed at 160 °C under different isobaric saturation conditions of supercritical $CO_2$ (10, 14 and 18 MPa) [48, 49]. PC/SMA foams exhibit the polygon-closed-cell structures having pentagonal and hexagonal faces, which express the most energetically stable state of polygon cells. Such foam structure

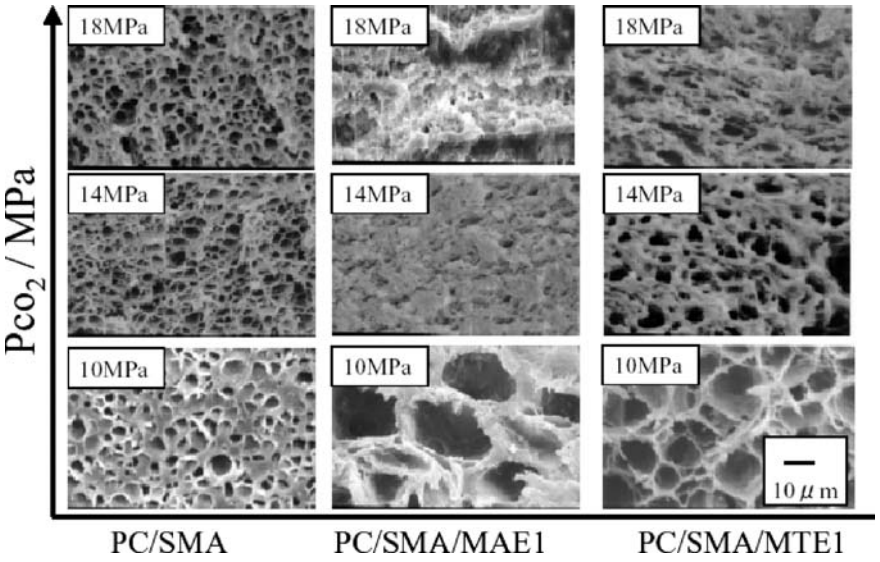


*Fig. 10. Typical SEM images of the fracture surfaces of PC-based nano-composites (PCCNs) and PC/SMA blend (without nano-filler) foamed under at 160 °C under different isobaric condition (10, 14 and 18 MPa)*

was obtained probably because these foams belong to the polymeric foams having high gas phase volume (> 0.6). Obviously, under low saturation $CO_2$ pressure (~ 10 MPa) both PCCN foams exhibit large cell size, indicating the dispersed clay particles hinder $CO_2$ diffusion by creating a maze or a more tortuous path as discussed in the literature [48]. However, high $CO_2$ pressure (~ 18 MPa) provides a large supply of $CO_2$ molecules, which can subsequently form a large population of cell nuclei upon depressurization. The PC/SMA/MAE1 (*syn*-FH-$C_{18}$TM) (OMLF = 1 wt.%) foam shows smaller cell size, i. e., larger cell density compared to PC/SMA foam, suggesting that the dispersed clay particles act as nucleating sites for cell formation and lowering of d with clay. The incorporation of nanoclay hinders $CO_2$ diffusion and simultaneously induces heterogeneous nucleation because of a lower activation energy barrier compared to homogeneous nucleation [50]. They conducted the characterization of the interfacial tension between bubble and matrix by using modified classical nucleation theory [51].

| Systems | | $\gamma\, S(\theta)^{1/3}$ mJ/m$^2$ | S(θ) |
|---|---|---|---|
| PC/SMA-$CO_2$ | $Pco_2$ = 10 MPa | 10.7 | 1.0 |
| PC/SMA/MAE1-$CO_2$ | | 8.6 | 0.53 |
| PC/SMA/MAE2.5-$CO_2$ | | 8.0 | 0.42 |
| PC/SMA-$CO_2$ | $Pco_2$ = 14 MPa | 10.9 | 1.0 |
| PC/SMA/MAE1-$CO_2$ | | 9.7 | 0.72 |
| PC/SMA/MAE2.5-$CO_2$ | | 9.9 | 0.77 |
| PC/SMA-$CO_2$ | $Pco_2$ = 18 MPa | 13.6 | 1.0 |
| PC/SMA/MAE1-$CO_2$ | | 10.2 | 0.42 |
| PC/SMA/MAE2.5-$CO_2$ | | 9.2 | 0.30 |
| PC/SMA-$CO_2$ | $Pco_2$ = 22 MPa | 11.3 | 1.0 |
| PC/SMA/MAE1-$CO_2$ | | 12.4 | – |
| PC/SMA/MAE2.5-$CO_2$ | | 8.0 | 0.36 |

*Table 2. Interfacial tension ($\gamma S(\theta)^{1/3}$) including energy reduction factor ($S(\theta)$) of systems [49]*

In Table 2, the interfacial tension and energy reduction factor of systems are summarized [49]. The interfacial tension of PC/SMA/MAE1 (including energy reduction factor S(θ) factor) and PC/SMA (S(θ) = 1) are 9.7 mJ/m$^2$ and 10.9 mJ/m$^2$ at 14 MPa, respectively. These estimated values of γ are in good agreement with that of other poly(methyl methacrylate) (PMMA)-$CO_2$ system (10 to 20 mJ/m$^2$) [52]. The interfacial tension slightly decreases with increasing in clay content under same $CO_2$ pressure condition, indicating heterogeneous cell nucleation occurs easily with increasing in clay content. The estimated reduction factor (S(θ) = 0.3 to 0.8) is the same order compared with the foaming of PLA-based nanocomposites [53].

Fig. 11 shows the cell size (d), the cell density ($N_c$) and the mean cell wall thickness (δ) relations of the nanocomposite foams obtained by a series of their recent studies [49, 53, 54]. In the case of nanocomposite foams, the cell wall thickness becomes 2 to 6 times compared to that of neat polymer foams due to the spherical cell shape caused by the high modulus of the materials during processing. The controlled structure of the nanocomposite foams is from microcellular ($d \cong 20$ μm and $N_c \cong 1.0 \times 10^9$ cell · cm$^{-3}$) to nanocellular ($d \cong 200$ nm and $N_c \cong 1.0 \times 10^{14}$ cell · cm$^{-3}$).

More detailed surveys on various types of nano-composite foaming can be also available in the literatures [55 to 58].

### *4.2 Electrospinning Processing*

Fibers and nanofibers of N6CN (diameter of 100 to 500 nm) were electrospun from 1,1,1,3,3,3-hexafluoro-2-propanol (HFIP) solution and collected as non-woven fabrics or as aligned yarns [59]. The electrospinning process resulted in highly aligned MMT particles and PA 6 crystallites. The cylindrical shaped fibers and nanofibers, ribbon shaped fibers were also found in the products (see Fig. 12). Using polystyrene (PS)/MMT and poly(methyl methacrylate) (PMMA)/MMT nano-composite solutions, the same approach is conducted [60, 61]. The fiber diameters of PS-based nano-composite were adjusted from 4 μm to 150 nm by changing the tetra-

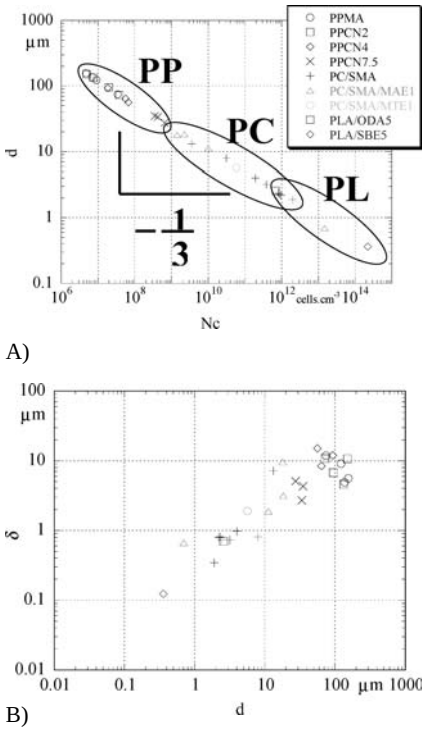


*Fig 11. Cell size versus cell density (A) and (B) cell wall thickness (δ) versus cell size for PCCN systems. For the comparison, here we show other nanocomposite foams obtained by a series of our recent studies [48, 53]; PP: polypropylene-based , PLA: polylactide-based nanocomposite foams*

hydrafuran (THF) and dimethylformamide (DMF) solution concentration (see Fig. 13). The addition of MMT to the spinning solution produced fibers with a highly aligned MMT layer structure at low MMT content (4 wt.%). The agglomerated tactoids of MMT were observed at higher concentration. The shear modulus of fiber was enhanced and the glass transition temperature was increased by 20 °C due to the MMT dispersion. Electrospinning can be expected to align other nanofillers such as carbon nanotubes.

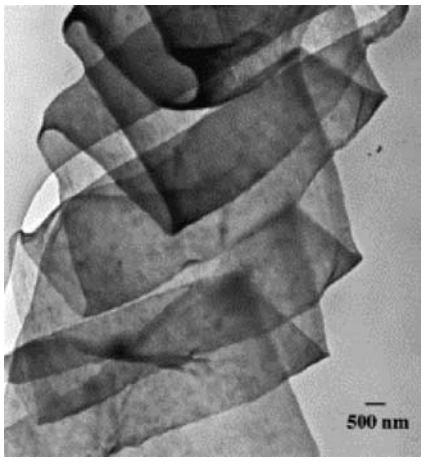


*Fig. 12. TEM micrograph of a ribbon shaped nanofiber [59]*

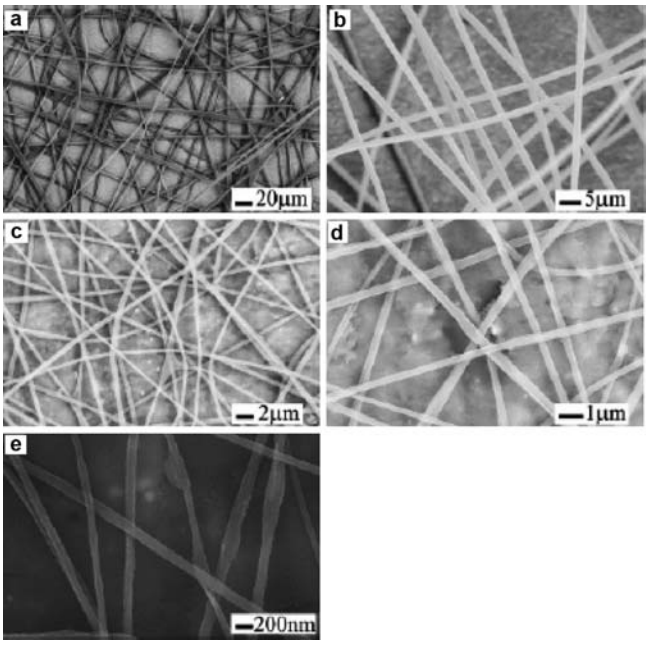


*Fig. 13. SEM images of electrospun PS fibers with 4 wt.% MMT at different PS concentration: (a) 20 wt.%, (b) 15 wt.%, (c) 10 wt.%, (d) 7.5 wt.%, and (e) 5 wt.% [60]*

## 5 Conclusions

The potential of nano-composites in various sectors of research is promising. The PLFNCs offer attractive potential for diversification and application of conventional polymeric materials. A significant amount of work has already been done on various aspects of PLFNCs [1], in order to understand structure development-property relationship in various PLFNCs. PLFNCs are already commercially available and applied in industrial products. The major impact will be at least a decade away.

## References

1 *Ray, S. S., Okamoto, M.:* Prog. Polym. Sci. 28, p. 1539 (2003)
2 *Usuki, A., Kojima, Y., Okada, A., Fukushima, Y., Kurauchi, T., Kamigaito, O.:* J. Mater. Res. 8, p. 1174 (1993)
3 *Gao, F.:* Materials Today 7, p. 50 (2004)
4 *Usuki, A., Hasegawa, N., Kato, M.:* Adv. Polym. Sci. 179, p. 135 (2005)
5 U.S. Patent No. 2531396 (1950) National Lead Co.
6 U.S. Patent No. 3084117 (1963) Union Oil Co.
7 Japanese Kokai Patent Application No. 109998 (1976) Unitika Ltd.
8 *Fukushima, Y., Inagakim S.:* J. Incl. Phen. 5, p. 473 (1987)
9 *Kojima, Y., Usuki, A., Kawasumi, M., Okada, A., Fukushima, Y., Karauchi, T., Kamigaito, O.:* J. Mater. Res. 8, p. 1185 (1993)
10 *Jose-Yacaman, M., Rendon, L., Arenas, J., Puche, M. C. S.:* Science 273, p. 223 (1996)
11 *Vaia, R. A., Ishii, H., Giannelis, E. P.:* Chem. Mater. 5, p. 1694 (1993)
12 *Vaia, R. A., Giannelis, E. P.:* Macromolecules 30, p. 7990 (1997)
13 *Vaia, R. A., Giannelis, E. P.:* Macromolecules 30, p. 8000 (1997)
14 *Hiroi, R., Sinha Ray, S., Okamoto, M., Shiroi, T.:* Macromol. Rapid Commun. 25, p. 1359 (2004)
15 *Lagaly, G.:* Clay Miner. 16, 1 (1970)
16 *Vaia, R. A.:* Teukolsky RK, Giannelis EP, Chem. Mater. 6, p. 1017 (1994)

17 *Li, Y. Q., Ishida, H.:* Langmuir 19, p. 2479 (2003)
18 *Osman, M. A.:* J. Mater. Chem. 16, p. 3007 (2006)
19 *Paul, D. R., Zeng, Q. H., Yu, A. B., Lu, G. O.:* J. Colloid Interface Sci. 292, p. 462 (2005)
20 *Yoshida, O., Okamoto, M.:* Macromol. Rapid Commun. 27, p. 751 (2006)
21 *Saito, T., Okamoto, M.:* Macromol. Mater. Eng. in press (2006)
22 *Totha, R., Coslanicha, A., Ferronea, M., Fermeglia, M., Pricl, S., Miertus, S., Chiellini, E.:* Polymer 45, p. 8075 (2004)
23 *Sinsawat, A., Anderson, K. L., Vaia, R. A., Farmer, B. L.:* J. Polym. Sci. Part B: Polym. Phys. 41, p. 3272 (2003)
24 *Kuppa, V., Menakanit, S., Krishnamoorti, R., Manias, E.:* J. Polym. Sci: Part B: Polym. Phys. 41, p. 3285 (2003)
25 *Zeng, Q. H., Yu, A. B., Lu, G. Q., Standish, R. K.:* Chem. Mater. 15, p. 4732 (2003)
26 *Sheng, N., Boyce, M. C., Parks, D. M., Rutledge, G. C., Abes, J. I., Cohen, R. E.:* Polymer 45, p. 487 (2004)
27 *Zerda, A. S., Caskey, T. C., Lesser, A.:* Macromolecules 36, p. 1603 (2003)
28 *Zhao, Q., Samulski, E. T.:* Macromolecules 36, p. 6967 (2003)
29 *Yang, K., Ozisik, R.:* Polymer 47, p. 2849 (2006)
30 *Lee, E. C., Mielewski, D. F., Baird, R. J.:* Polym. Eng. Sci. 44, p. 1773 (2004)
31 *Zhao, L., Li, J., Guo, S., Du, Q.:* Polymer 47, p. 2460 (2006)
32 *Shao, W., Wang, Q., Li, K.:* Polym. Eng. Sci. 45, p. 451 (2005)
33 *Okamoto, M., Nam, P. H., Maiti, P., Kotaka, T., Hasegawa, N., Usuki, A.:* Nano Lett. 1, p. 295 (2001)
34 *Okamoto, M.:* Polymer/ Layered Silicate Nanocomposites, Rapra Review Report No 163. Rapra Technology, London (2003)
35 *Maiti, P., Okamoto, M.:* Macromole. Mater. Eng. 288, p. 440 (2003)
36 *Nam, P. H.:* Master Thesis, Toyota Technological Institute, Nagoya, Japan (2001)
37 *Sinha Ray, S., Okamoto, K., Okamoto, M.:* Macromolecules 36, p. 2355 (2003)
38 *Kojima, Y., Usuki, A., Kawasumi, M., Okada, A., Kurauchi, T., Kamigaito, O., Kaji, K.:* J. Polym. Sci. Part B: Polym. Phys. 33, p. 1039 (1995)
39 *Yalcin, B., Cakmak, M.:* Polymer 45, p. 2691 (2004)
40 *Medellin-Rodriguez, F. J., Burger, C., Hsiao, B. S., Chu, B., Vaia, R. A., Phillips, S.:* Polymer 42, p. 9015 (2001)
41 *Lele, A., Mackley, M., Galgali, G., Ramesh, C.:* J. Rheol. 46, p. 1091 (2002)
42 *Bafna, A., Beaucage, G., Mirabella, F., Mehta, S.:* Polymer 44, p. 1103 (2003)
43 *Roe, R.:* Methods of X-ray and neutron scattering in polymer science. Oxford University Press, New York (2000)
44 *Bafna, A., Beaucage, G., Mirabella, F., Skillas, G., Sukumaran, S.:* J. Polym. Sci., Part B: Polym. Phys. 39, p. 2923 (2001)
45 *van Olphen, H.:* An Introduction to Clay Colloid Chemistry. Wiley, New York (1977)
46 *Okamoto, M., Nam, P. H., Maiti, M., Kotaka, T., Nakayama, T., Takada, M., Ohshima, M., Usuki, A., Hasegawa, N., Okamoto, H.:* Nano Lett. 1, p. 503 (2001)
47 *Nam, P. H., Okamoto, M., Maiti, P., Kotaka, T., Nakayama, T., Takada, M., Ohshima, M., Hasegawa, N., Usuki, A.:* Polym. Eng. Sci. 42(9), p. 1907 (2002)
48 *Mitsunaga, M., Ito, Y., Okamoto, M., Sinha Ray, S., Hironaka, K.:* Macromol. Mater. Eng. 288, p. 543 (2003)
49 *Ito, Y., Yamashita, M., Okamoto, M.:* Macromol. Mater. Eng. 291, p. 773 (2006)
50 *Klempner, D., Frisch, K. C.:* Handbook of Polymeric Foams and Foam Technology. Hanser, Munich Vienna (1991)
51 *Colton, J. S., Suh, N. P.:* Polym. Eng. Sci. 27, p. 485 (1987)
52 *Goel, K., Beckman, E. J.:* Polym. Eng. Sci. 34, p. 1137 (1994)
53 *Ema, Y., Ikeya, M., Okamoto, M.:* Polymer 47, p. 5350 (2006)
54 *Fujimoto, Y., Sinha Ray, S., Okamoto, M., Ogami, A., Ueda, K.:* Macromol. Rapid Commun. 24, p. 457 (2003)
55 *Lee, L. J., Zeng, C., Cao, X., Han, X., Shen, J., Xu, G.:* Composites Science and Technology 65, p. 2344 (2005)
56 *Cao, X., Lee, L. J., Widya, T., Macosko, C.:* Polymer 46, p. 775 (2005)
57 *Chandra, A., Gong, S., Turng, L.-S., Gramann, P., Cordes, H.:* Polym. Eng. Sci. 45, p. 52 (2005)
58 *Strauss, W., D'Souza, N. A.:* J. Cellular Plastics 40, p. 229 (2004)
59 *Fong, H., Liu, W., Wang, C. S., Vaia, R. A.:* Polymer 43, p. 775 (2002)
60 *Ji, Y., Li, B., Ge, S., Sokolov, J. C., Rafailovich, M. H.:* Langmuir 22, p. 1321 (2006)
61 *Wang, M., Hsieh, A. J., Rutledge, G. C.:* Polymer 46, p. 3407 (2005)

*Date received: February 1, 2006*
*Date accepted: July 21, 2006*

You will find the article and additional material by entering the document number **IPP0012** on our website at *www.polymer-process.com*